IMPACT DAMAGE AND REPAIR OF COMPOSITE STRUCTURES (GARTEUR ACTION GROUP - 28)

B. G. Falzon
Imperial College London, Department of Aeronautics,
South Kensington Campus, London, SW7 2AZ
United Kingdom

OVERVIEW

The primary objective of GARTEUR (Group for Aeronautical Research and Technology in Europe) Action Group – 28 was to develop and validate analytical and numerical methods to characterise real impact damage in composite structures, particularly those designed to sustain load in a postbuckled state, and to study the durability of bonded repairs. The consortium had partners from ONERA, EADS-CCR (France), DLR, AIRBUS-Deutschland, EADS-M (Germany), CIRA (Italy), INTA (Spain), SICOMP, SAAB, (Sweden), NLR (The Netherlands), QinetiQ, BAE Systems, Imperial College London and the University of Sheffield (United Kingdom). The Action Group tasks were divided into four Work Elements (WEs): WE1-Prediction and characterisation of impact damage, WE2-Postbuckling with delamination, WE3-Repair and WE4-Fatigue. This paper outlines the main developments and achievements within each Work Element.

1. INTRODUCTION

Advanced carbon-fibre composite material is being increasingly utilised in civil and military primary aerostructures because of its superior specific weight and stiffness properties. However, these structures are sensitive to low-velocity impact, which may create multiple delaminations through the thickness, as well as matrix cracking and fibre breakage. To date, no reliable and fully validated analytical tool, able to predict damage initiation and propagation, has been developed. This response is further complicated in postbuckling structures where the resulting deformations give rise to dramatic increases in interlaminar shear and through-thickness stresses in critical regions. In many cases, damage growth is difficult to predict reliably and aviation authorities have adopted a "no-growth" criterion as part of the certification requirements. This results in the need to perform a large amount of testing, which is very expensive and time consuming. Another aspect is that structures must be repaired when subjected to low velocity impact and that the efficiency of bonded repairs to composite structures must be studied.

Previous research work[1-3] has shown that understanding low energy impact damage is critical for damage tolerance of composite structures. It may create superimposed delaminations at the layer interfaces and the material is often repaired by bonding. The durability and the efficiency of a bonded repair to the parent composite structure, subjected to loading appropriate to realistic operating conditions, becomes crucial.

Industry therefore shows a clear interest in the development of methodologies that will permit to address this problem in a cost-efficient way. In recognition of the need to reduce testing costs and to develop reliable prediction methods for repaired structures under fatigue loading, the following objectives were defined:

- predict and characterise impact damage (type, size, geometry, and constitutive properties etc.),
- analyse panels with impact damage, which are designed for postbuckling,
- study the durability of bonded repairs to composite structures subjected to low energy impact,
- develop, improve and validate fatigue prediction codes as part of an integrated safety-engineering concept (both for damaged panels and repaired panels).

1.1 General Considerations

The primary objective of the Action Group was to develop and validate methods, which are able to characterise real impact damage in composite structures and to study the durability of bonded repairs under fatigue loading. The program was divided into four Work Elements, each of them with a Work Element Leader responsible for the final reporting of the corresponding Work Element. A fifth Work Element was also included as a means of assigning the task of compiling the Final Report and Executive Summary.

The primary aim of Work Element 1 (WE-1) was to define typical impact threats, describe and model the resulting damage and develop improved methods to predict the impact response and damage formation. Characterising impact damage is complex in that it involves irregular and multiple delaminations, extensive matrix cracks, fibre fracture and initial imperfections such as dents and other shape distortions.

Work Element 2 (WE-2) focussed on the response of postbuckling stiffened composite panels with and without delaminations. The effect of the location of impact damage on panel failure was studied. Both damaged panels and repaired panels were considered and a great deal of effort was expended in assessing the robustness of the various finite element packages in capturing these high non-linearities.

The aim of Work Element 3 (WE-3) was to produce a validated method for assessing repair reliability of composite panels under fatigue and static loading. A number of experimental and numerical studies were also performed.

Work Element 4 (WE-4) was dedicated to the issue of fatigue in primary aerostructures. In general, these structures are not considered to be fatigue critical but fatigue certification results in the need to perform a large amount of tests, which is costly and time consuming. Many structures have been tested and no fatigue failure has occurred. However, this study aimed to assess whether this superior fatigue performance remained for impact-damaged structures.

A considerable amount of research was conducted by all partners involved and this paper can only highlight some of the main results achieved throughout this four-year programme. The reader is referred to the Technical Report[4] for further details.

2. WE-1: PREDICTION AND REPAIR OF COMPOSITE STRUCTURES

2.1 Introduction

If composites structures are to gain wider acceptance in aerospace applications, their response to impact damage and their subsequent ability to carry load (i.e. damage tolerance) should be fully understood. These structures are particularly susceptible to impact damage caused by dropped tools during maintenance routines, structural damage which may arise during manufacturing or assembly, damage caused by service vehicles, hail and runway debris. Figure 1 shows the resulting damage on the canard of a SAAB 39 Gripen fighter from a service vehicle door.

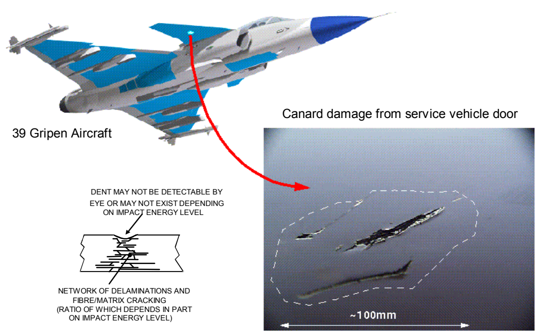

FIG. 1: Damage on canard of a 39 Gripen fighter aircraft.

2.2 Dynamic impact on plates (IMPERIAL - UK)

An analytical solution for delamination onset under small mass, high velocity impact was developed by Olsson[3] and given in Equation 1.

$$(1)\quad F_{d1}^{dyn} \approx 1.21 F_{d1}^{stat} = 1.21\pi\sqrt{32 G_{IIc} D/3}$$

where F_{d1}^{dyn} is the dynamic force at delamination onset, F_{d1}^{stat} is the static force for delamination onset, $D = Q_b h^3/12$ ($Q_b = E_r/\left(1-\nu_r^2\right)$, were E_r and ν_r are the stiffness and Poisson's ratio in the radial direction, respectively) and G_{IIc} is the critical strain energy release rate in mode II. It is shown that the dynamic force required to initiate delamination was approximately 21% higher than that required to cause delamination under quasi-static conditions. Good accuracy was achieved in comparison with dynamic explicit finite element results over a range of orthotropic plate thicknesses as shown in Figure 2.

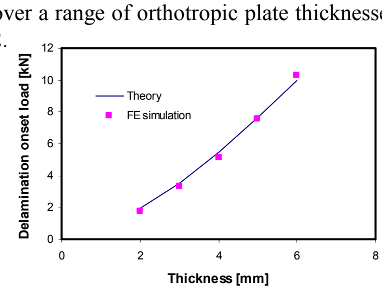

FIG. 2: Delamination onset load versus plate thickness.

2.3 Impact damage in sandwich panels (SICOMP-SWEDEN)

This study investigated the compression-after-impact (CAI) strength of sandwich panels with non-crimp-fabric (NCF) face-sheets. Figure 3 shows two C-scan images of impacted panels. The image on the left is a C-scan image of a panel with Barely Visible Impact Damage (BVID). This panel had NCF face-sheets with a lay-up of $[0/90/\pm45]_S$ and a core made from Divinycell H80 with a density of 80 kg/m^3. The second panel shown on the right had identical face-sheets but with a higher-density core (Divinycell H200 - 200 kg/m^3). The resulting damage, due to impact, in the face-sheets was found to be very similar to that caused by impact on monolithic panels made of NCF. In assessing the CAI strength, it was observed that kink-bands formed and propagated around the point of impact leading to failure. A simplified notch-type failure model was proposed to predict CAI strength in BVID specimens. The length of the notch was approximated by the length of the projected delamination from the C-scan images.

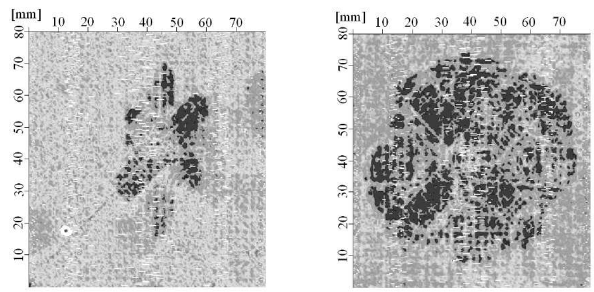

FIG. 3: C-scan images of impacted NCF sandwich panels.

2.4 Finite element predictions of impact response (INTA-SPAIN)

A finite element analysis, to simulate the impact event, was undertaken in MSC Marc, an implicit non-linear code. The following failure modes where considered: Fibre fracture, fibre microbuckling, matrix failure in tension, compression and shear, failure by peeling stresses and failure by interlaminar shear stress. A maximum stress criterion was used for each failure mode. When a particular component of the stress tensor at a particular ply reached a maximum allowable value, the corresponding stiffness was reduced to zero and the analysis continued.

The impactor was modelled as a rigid spherical surface, under gravity, and solid composite elements were used to model the plate. The impactor was initially placed above the panel at the experimental drop-height with zero initial velocity. The finite element model is shown in Figure 4.

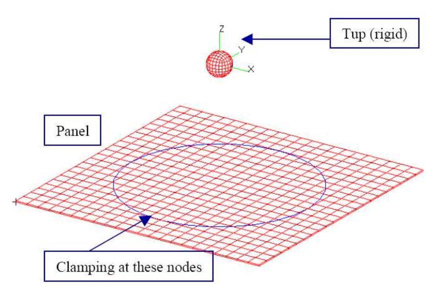

FIG. 4: Finite element model of plate and impactor.

Failure indices associated with each failure mode may be plotted with MSC/Marc for each ply within a particular solid composite element. Since the experimental damaged area scans did not distinguish bertween the different types of failure (delaminations, matrix cracks, fibre fracture), the correlation between the tests and finite element analysis results were made for the overall damaged area defined by all elements which have undergone some type of damage within one or more plies. One set of results is shown in Figure 5 for a panel made from IM7/8552 unidirectional pre-impregnated composite tape subjected to a medium-velocity impact.

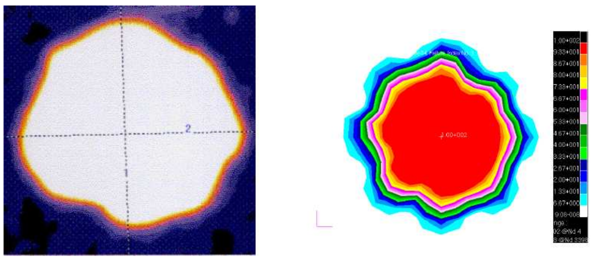

FIG. 5: Comparison of C-scan image with predicted damage area.

The study showed that the prediction of the damaged area was quite satisfactory for material IM7/8552 but marginally so for another material that was used for another set of panels (IM7/977-2). This was attributed to the through-thickness allowable strength value which was obtained from literature sources. The numerical modelling was found to be very sensitive to this parameter. The deflection-time plots for the response of these two types of panels for both low and medium velocity impact are shown in Figures 6 and 7.

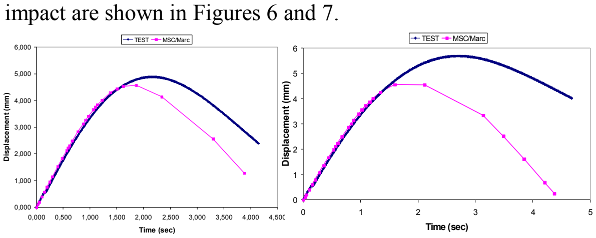

IM7/977-2 IM7/8552

FIG. 6: Deflection-time graphs for low-velocity impact.

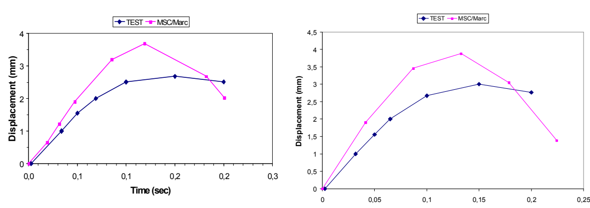

IM7/977-2 IM7/8552

FIG. 7: Deflection-time graphs for medium-velocity impact.

As is evident, the correlation is, at best, fair and better material modelling characterisation is required. The initial response for low-velocity impact shows good correlation although this is not the case for medium-velocity impact.

2.5 Fast finite element analysis of impact damage (DLR - GERMANY)

An in-house simplified finite element tool (CODAC) was developed by DLR for the rapid prediction of BVID to low-energy impact. The impactor was idealised as a point mass and coupled to the structure using a Hertzian indentation law. An implicit Newmark time stepping scheme[5] was used for the analysis. Shell elements, adapted to model either monolithic or sandwich structures, were implemented. A damage mechanics approach was adopted by using the Choi/Chang failure criterion[6] to model delamination, a simplified form of the Hashin criterion[7] for in-plane matrix failure and a maximum stress criterion for fibre breakage. The corresponding stiffness terms were degraded to zero when the critical stress-states were reached.

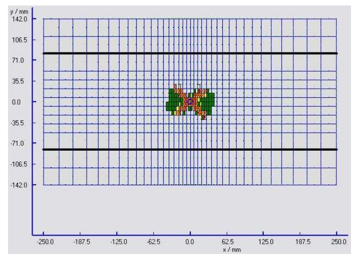

FIG. 8: Predicted damage due to 50J impact.

Figure 8 shows the projected damage of a plate subjected to a 50J impact. Red indicates fibre fracture, white areas are delaminations, green areas contain matrix cracks and yellow denotes both matrix cracks and delamination. Figure 9 shows the force versus time response for a 1J impact (BVID) on a sandwich structure. When the core stiffness terms were degraded to 0.1 of their initial values, good correlation was achieved with experimental results for the initial response and first occurrence of damage through core-crushing. Figure 10 shows the extent of damage predicted and the curved solid blue line indicates the projected damage area observed experimentally.

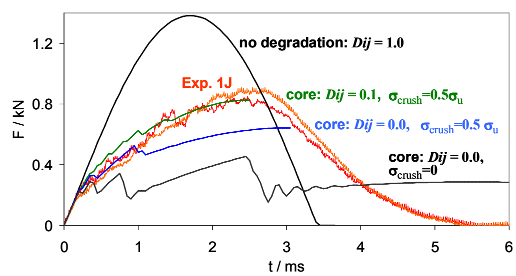

FIG. 9: Predicted damage due to 50J impact.

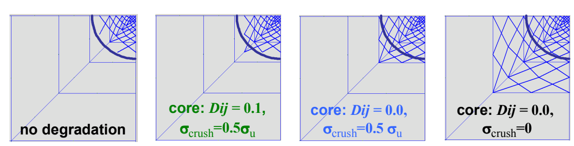

FIG. 10: Predicted damage due to 50J impact.

2.6 Concluding remarks for Work Element 1

A number of experimental studies, undertaken by different partners within the consortium, have yielded new insight into the complex damage mechanisms arising from impact. Analytical and numerical tools have been developed for predicting the response of monolithic and sandwich composite structures to Barely Visible Impact Damage (BVID).

3. WE-2: POSTBUCKLING WITH DELAMINATION

3.1 Introduction

Numerous experimental studies have shown the ability of stiffened composite panels to sustain loading beyond initial skin-buckling[8-10]. The primary aim of this Work Element was to assess, and further develop, the current numerical capability of modelling the response of postbuckling stiffened composite panels containing delaminations. To validate the various numerical strategies adopted, a set of experimental benchmarks were compiled and distributed to all partners[11]. These panels are described in Table 1.

TAB. 1: Database of panel tests.

Panel ID	Testing Lab	Description
FALZON-1	Imperial College London	Blade-Stiffened, undamaged, secondary bonded
FALZON-2	Imperial College London	I-Stiffened, undamaged, secondary bonded
EADS-M	EADS-M	Blade-Stiffened, undamaged, secondary bonded
SFN-1	QINETIQ	I-Stiffened, impact damaged, secondary bonded
SFN-2	QINETIQ	I-Stiffened, impact damaged, secondary bonded
SFN-3	QINETIQ	I-Stiffened, impact damaged, secondary bonded
SFN-4	QINETIQ	I-Stiffened, impact damaged, secondary bonded
SFN-5	QINETIQ	I-Stiffened, undamaged, secondary bonded

3.2 Modelling delamination using VCCT (INTA-SPAIN)

A stiffened panel (SFN-3) was modelled using shell (CQUAD4) elements (Figure 11). The adhesive bond at the skin/stiffener interface was modelled using rigid beam elements (RBAR). Embedded defects in the skin were modelled using contact elements (CGAP) in MSC/NASTRAN. A Modified Virtual Crack Closure Technique[12] (MVCCT) was used to predict the onset of delamination propagation. This was predicted to within 3%. A model of a pristine panel was also developed using solid (HEXA8) elements to predict skin-stiffener separation. A stress-based failure criterion could not accurately predict failure loads and both models failed to capture secondary instabilities reliably.

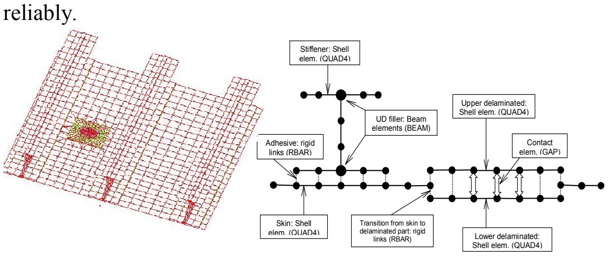

FIG. 11: Finite element plate model of panel SFN-3.

3.3 Non-linear solution schemes for modelling postbuckling panels (ONERA-FRANCE)

Three numerical strategies were implemented in an in-house finite element code to assess their robustness in capturing the highly non-linear response of postbuckling structures:

(1) Newton-Raphson and Arc-Length schemes[13]: these were unable to trace a stable solution path beyond the secondary instability (mode-jump).

(2) Eigenmode injection[14]: This uses the schemes in (1) but at the bifurcation point, the associated eigenmodes (corresponding to negative eigenvalues of the tangential stiffness matrix) are scaled and added to the current displacement. This method was found to be very sensitive to the load increment used near critical points on the equilibrium path.

(3) Implicit dynamic scheme (Newmark)[5]: This method was robust but oscillations were difficult to damp out beyond the mode-jump. Results for panel FALZON-1, using this method, are shown in Figure 12.

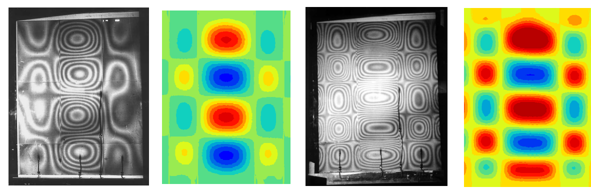

FIG 12: Experimental and FEA comparison.

3.4 An automated hybrid procedure for capturing mode-jumping (IMPERIAL-UK)

Most non-linear implicit solution schemes fail to reliably predict secondary instabilities in highly postbuckled stiffened composite panels. These are characterised by mode-jumps (sudden changes in the postbuckling mode-shape) and represented by secondary bifurcation points on an equilibrium path as shown in Figure 13. Experimental evidence exists to show that this energy-dissipating phenomenon may cause failure in vulnerable postbuckling structures[10, 15]. A robust and efficient strategy, which utilises an automated quasi-static pseudo-transient hybrid scheme was implemented in an in-house finite element code. The solution utilised a standard implicit quasi-static scheme (Newton-Raphson/Arc-length) whilst the tangential stiffness matrix, K_t , was positive definite. A critical point was detected when an entry in the diagonal matrix, D, of the factored $K_t=L^TDL$, became negative. A 'bracketing procedure' was used to locate the critical point more accurately. A load increment just above this point and a displacement increment based on the eigenmode close to this critical point were used as initial conditions the pseudo-transient solution scheme. This scheme involved a modified form of explicit dynamic analysis where near-critical damping is obtained at the mode-jump[16]. During this transient phase the following equations were solved using explicit dynamic analysis:

$$
\begin{aligned}
{}^{t+\Delta t}\dot{u} &= \bar{K}_t^{-1}\left({}^{t+\Delta t}\lambda f_{ext} - {}^{t}K_t\,{}^{t}u\right) \\
{}^{t+\Delta t}u &= \left(1+\frac{\Delta t}{2}\right){}^{t}\dot{u} + \frac{\Delta t}{2}\,{}^{t+\Delta t}\dot{u}
\end{aligned}
\qquad (2)
$$

f_{ext} :fixed external load vector
u :displacement vector
$\dot{u}$:velocity vector
$\bar{K}_t$:previous estimate of tangential stiffness matrix
λ :load multiplier
Δt :time step

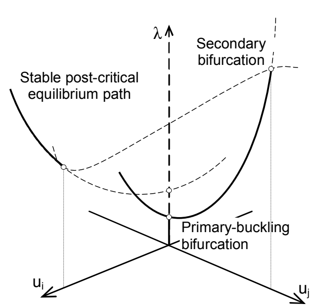

FIG. 13: Equilibrium paths.

Figure 14 shows a comparison between theory and experiment for panel FALZON-2. With reference to Figure 15, it is noted that the initial mode-jump was captured with good accuracy. The second mode-jump, for PANEL-2, was predicted to occur at a loading which was 13.8% higher than that observed experimentally. This was attributed to the considerable extent of matrix microcracking which was not accounted for in the present finite element modelling.

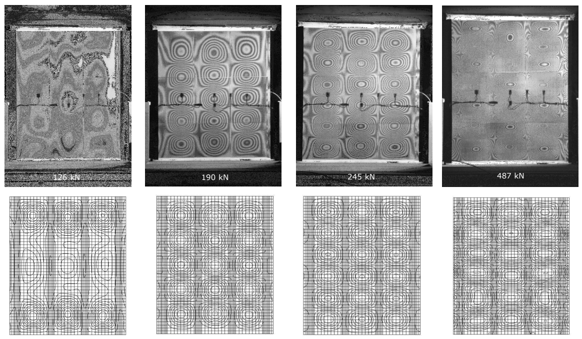

FIG. 14: Comparison between experiment and FEA for panel FALZON-2.

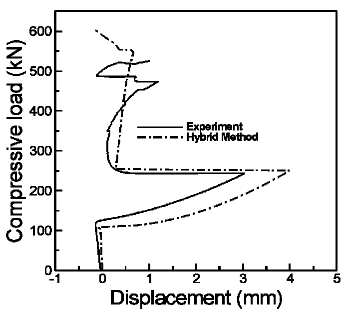

FIG. 15: Out-of-plane displacement at centre of panel FALZON-2.

3.5 Modelling postbuckling panels with embedded delaminations (CIRA - ITALY)

The VCCT was also adopted in this study of delamination growth. This particular formulation included all degrees-of-freedom (displacements and rotations) with eight-node shell elements. It provided preferable constraints, yielding accurate strain energy release rates (SERR). With reference to Figure 16, the equations to calculate the SERR, for a corner node, j, are:

(3)

$$G_I = -\frac{1}{2B_j\Delta}\left\{\begin{array}{l}\left[\begin{array}{l}F_{z_j}\left(w_q - w_{q'}\right) + F_{z_e}\left(w_l - w_{l'}\right) + M_{x_j}\left(\theta_{x_q} - \theta_{x_{q'}}\right) + \\ +M_{x_e}\left(\theta_{x_l} - \theta_{x_{l'}}\right) + M_{y_j}\left(\theta_{y_q} - \theta_{y_{q'}}\right) + M_{y_e}\left(\theta_{y_l} - \theta_{y_{l'}}\right)\end{array}\right] + \\ +\left[\frac{1}{2}F_{z_i}\left(w_p - w_{p'}\right) + \frac{1}{2}M_{x_i}\left(\theta_{x_p} - \theta_{x_{p'}}\right) + \frac{1}{2}M_{y_i}\left(\theta_{y_p} - \theta_{y_{p'}}\right)\right] + \\ +\left[\frac{1}{2}F_{z_k}\left(w_r - w_{r'}\right) + \frac{1}{2}M_{x_k}\left(\theta_{x_r} - \theta_{x_{r'}}\right) + \frac{1}{2}M_{y_k}\left(\theta_{y_r} - \theta_{y_{r'}}\right)\right]\end{array}\right\}$$

$$G_{II} = -\frac{1}{2B_j\Delta}\left[F_{x_j}\left(u_q - u_{q'}\right) + F_{x_e}\left(u_l - u_{l'}\right) + \frac{1}{2}F_{x_i}\left(u_p - u_{p'}\right) + \frac{1}{2}F_{x_k}\left(u_r - u_{r'}\right)\right]$$

$$G_{III} = -\frac{1}{2B_j\Delta}\left\{\begin{array}{l}\left[F_{y_j}\left(v_q - v_{q'}\right) + F_{y_e}\left(v_l - v_{l'}\right) + M_{z_j}\left(\theta_{z_q} - \theta_{z_{q'}}\right) + M_{z_e}\left(\theta_{z_l} - \theta_{z_{l'}}\right)\right] + \\ \left[\frac{1}{2}F_{y_i}\left(v_p - v_{p'}\right) + \frac{1}{2}M_{z_i}\left(\theta_{z_p} - \theta_{z_{p'}}\right)\right] + \left[\frac{1}{2}F_{y_k}\left(v_r - v_{r'}\right) + \frac{1}{2}M_{z_k}\left(\theta_{z_r} - \theta_{z_{r'}}\right)\right]\end{array}\right\}$$

$$B_j = \frac{1}{2}\left[b_{j-1} + b_j\right]$$

A linear criterion was assumed for crack propagation:

(4) $$\left(\frac{G_I}{G_{IC}}\right) + \left(\frac{G_{II}}{G_{IIC}}\right) + \left(\frac{G_{III}}{G_{IIIC}}\right) = 1$$

where the subscript, C, denotes a critical value. Panel SFN-2, with an artificial delamination under the stringer foot (Figure 17), and panel SFN-3 with an artificial delamination in a skin-bay (Figure 18), were modelled using shell elements available in the commercial finite element code, ANSYS.

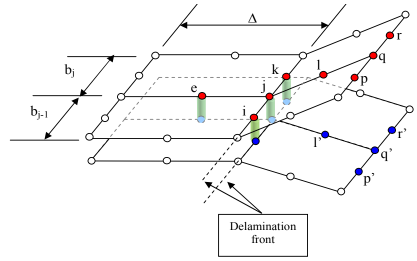

FIG. 16: Node sequence for VCCT.

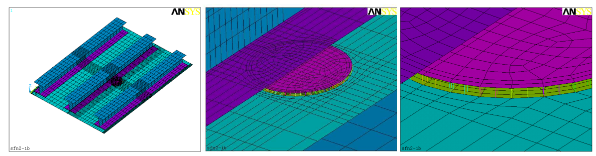

FIG. 17: Finite element model of panel SFN-2.

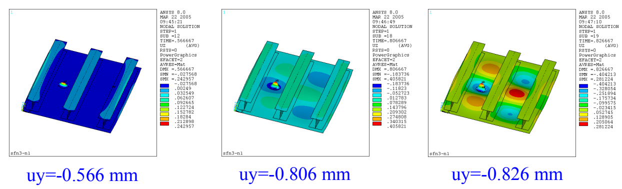

FIG. 18: Finite element model of panel SFN-3 showing local delamination buckling.

Up to the initial buckling load, no delamination growth was predicted for panel SFN-2. For panel SFN-3, local delamination buckling was observed and delamination growth was predicted perpendicular to the load direction.

3.6 Modelling embedded defects using cohesive elements (QINETIQ - UK)

Panel SFN-1 was modelled using ABAQUS and incorporating cohesive elements to capture delamination growth. Cohesive elements are characterised by a stress-relative displacement constitutive law with a high initial stiffness up to a critical stress, followed by a softening law as shown in Figure 19 for Mode I and Mode II/III. The area under this curve is a measure of the SERR for the creation of new crack surfaces. Complete decohesion occurs when a critical displacement is reached. This is usually dependent on the displacements on the individual modes and is derived from the assumed criterion used to propagate the crack. In this work, a linear law (Eq. 4) was assumed.

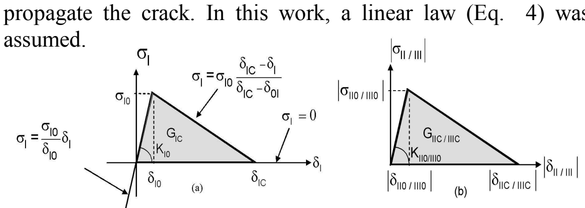

FIG. 19: Constitutive laws for interface element (a) Mode I and (b) Mode II/III.

These interface elements were inserted between plies where the delamination was expected to grow. Figure 20(a) shows the computed first buckling mode for the panel, which compares well with the Moiré fringe pattern obtained from experiment (Figure 20(d)). Figure 20(b) shows the local buckling of the delamination on the reverse side of the panel. Figure 20(c) shows the failure of the cohesive elements shown in red. In Figure 20(e) a comparison of out-of-plane displacements at the centre of the delamination indicates that the model predicts a similar trend but under-predicts the magnitude of displacement and the point at which global buckling occurs.

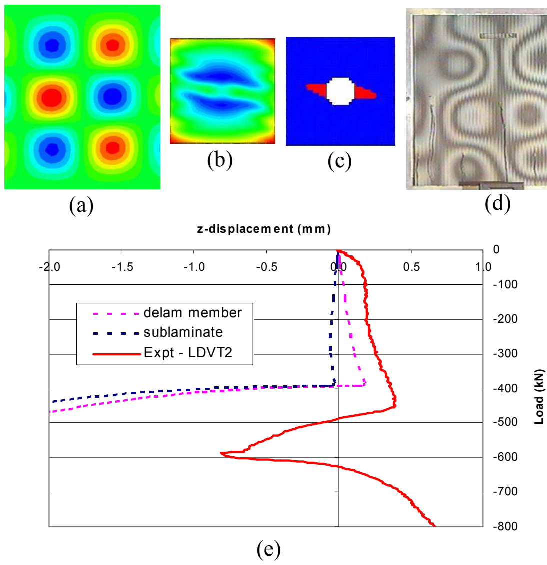

FIG. 20: Results for panel SFN-1.

3.6 Concluding remarks for Work Element 2

This work has presented a number of numerical strategies for modelling buckling and postbuckling stiffened composite panels with delaminations. The partners involved progressed on two fronts: (1) assessing the robustness of current non-linear algorithms and developing improved strategies (2) investigating numerical strategies for predicting initiation and propagation of delaminations.

4. WE-3: REPAIR

4.1 Introduction

Although it is well established that composite components in aerostructures offer significant advantages in strength and stiffness compared to metallic materials, they are susceptible to damage ranging from surface scratches, through delamination of plies, to complete perforation. The extent of damage determines the type of repair required. The more severe forms of damage are usually removed from the composite component and repaired, with the objective of restoring the component to its pristine strength and stiffness. Numerous studies have been undertaken[17-19], looking into repair schemes and investigating their response under static and fatigue loading, experimentally and computationally. In this Work Element, current bonded repair methodologies were presented and a number of tests, on repaired composite panels, were undertaken under static and fatigue loading.

4.2 Repair methodologies (BAE SYSTEMS - UK)

In-service repairs may be either permanent or temporary. Permanent repairs will typically restore the design ultimate strength and meet the requirements of fatigue loading, temperature and other environmental issues. If the repair fails to meet the acceptance criteria then it is considered temporary and must be monitored on a regular basis until a permanent repair is made. Figure 21 shows the sequence followed to determine the most suitable repair:

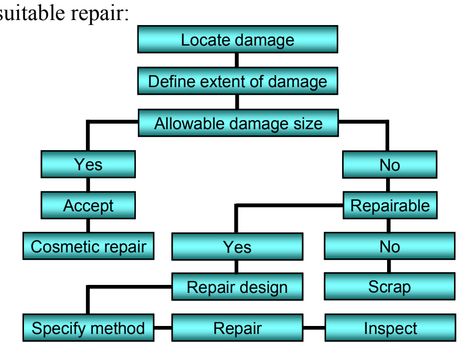

FIG. 21: Repair flow chart.

Figure 22 shows the types of repairs required, depending on the extent of damage. In a comprehensive series of test on repaired panels at room and hot/wet environments[17] no significant effect of hot/wet environmental conditioning (in distilled water at 50°C for 4 – 28 months) on the static and fatigue strength of repairs was observed. Under fatigue loading, the repaired panels did not perform nearly as well as the equivalent undamaged panels.

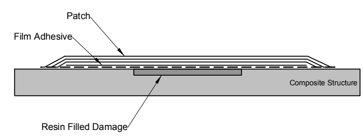

(a) Minor damage: damage up to 25 mm in diameter and 0.5 mm deep.

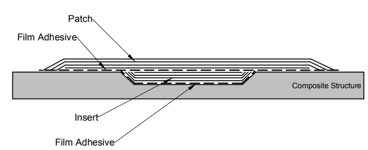

(b) Partial damage: damage up to 25 mm in diameter and more than 0.5 mm deep.

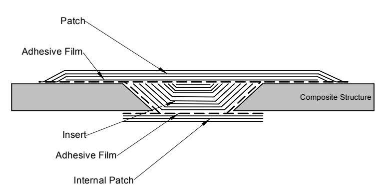

(c) Through-thickness damage.

FIG. 22: Types of repair.

The reliability and durability of bonded external patch repaired laminates for small through-thickness damage, loaded in compression at room temperature, has also been studied[20, 21]. The external patch technique is much simpler than the scarf approach but can only be used for a temporary repair until a permanent repair can be performed. It was shown that the patch thickness had no significant effect on the strength of the repaired panel but the introduction of the insert (plug) increased the failure load by approximately 20%. The effect of the insert was shown to reduce the stress concentration at the hole edge and further improve the performance. The optimum overlap length of the patch was 12.5 mm and it was shown that a high-stiffness patch produced higher peel and shear stresses. Radiography and scanning electron microscopy showed that the failure was due to patch debonding and microbuckling in the 0° plies surrounded by delamination and matrix cracking.

4.3 Repair of sandwich panels (SICOMP - SWEDEN)

A repair study on impacted sandwich panels with Non-Crimp Fabric (NCF) face-sheets was carried out. The core was restored by micro-balloon/epoxy filler and two repair schemes were investigated for the skin : a scarf and a step-joint as shown in Figure 23. Each step in the step-joint had a lay-up of (0/90/±45). The repaired panels were tested in compression and the results are shown on Table 2. It is seen that both repaired panels failed at approximately half the strain of that of the undamaged panel. The compression-after-impact (CAI) strength was improved. Failure for both panels was due to patch debonding and was attributed to the low L/t used. Digital Speckle Photogrammetry (DSP) revealed high strains at the edge of the patch as shown in Figure 24.

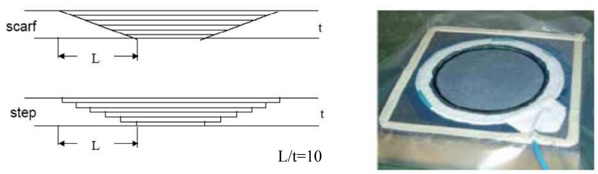

FIG. 23: NCF skin repairs: scarf and step joint repairs.

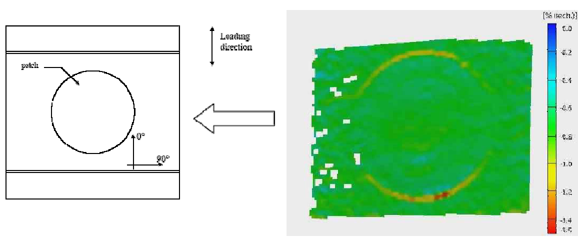

FIG. 24: Failure analysis - red indicates a highly strained region.

TAB. 2: Strain to failure

Panel	Failure strain
Undamaged	-1.18%
Impact damaged	-0.48%
Step joint repair	-0.62%
Scarf joint repair	-0.65%

This repair study also revealed that there were no significant differences in performance between the scarf and step-joint repairs for the NCF face-sheet sandwich panels.

4.4 Finite element analysis of BAE Systems test specimen (SAAB - SWEDEN)

The finite element package ABAQUS was used to model a scarf-joint repair specimen tested at BAE Systems. The test specimen is shown in Figure 25 and the finite element model is shown in Figure 26.

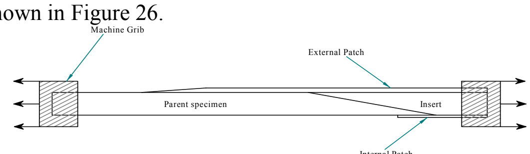

FIG. 25: BAE Systems test specimen.

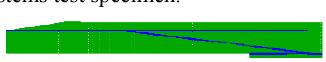

FIG. 26: Finite element model of scarf-joint repair specimen.

Static tension tests were simulated with material properties corresponding to room temperature and hot/wet (100°C/1.3% moisture content) conditions. SAAB were able reproduce, with good accuracy, the failure observed experimentally. Most specimens failed along the scarf bond-line and delamination was also observed within the external patch.

4.5 Stepped-joint repair analysis of woven laminate (IMPERIAL - UK)

The purpose of this programme was primarily to develop robust computational techniques for predicting the structural response of repaired woven laminates to static and fatigue loading[22]. These developments were validated against a set of experiments which were also conducted at Imperial College. A typical specimen is shown in Figure 27. The experimental results revealed that all specimens failed at the bond-line (Figure 28) and the repair efficiency was significantly degraded as shown in Figure 29.

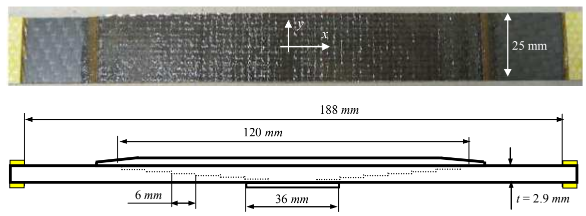

FIG. 27: Repair test specimen of woven laminate.

FIG. 28: Failed specimen under static tensile load.

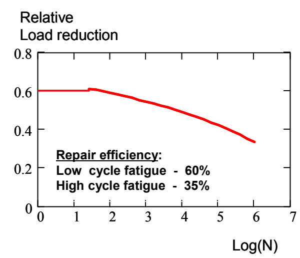

FIG. 29: Efficiency curves as a function of load cycles.

An in-house finite element code was developed which incorporated a number of novel numerical features. These included the use of a pseudo-transient formulation which was shown to be more stable than implicit non-linear schemes[23] and an interface element which included a fatigue-induced damage parameter.

A finite element model of a specimen tested under quasi-static conditions (Figure 27) is shown in Figure 30. Interface elements were placed at the bond-line (shown in red). Figure 31 shows the load versus end-displacement curve obtained from this model. It is seen that the damage accumulates gradually until catastrophic failure at a predicted loading of 25.5 kN. This was in excellent agreement with the range of loads obtained experimentally.

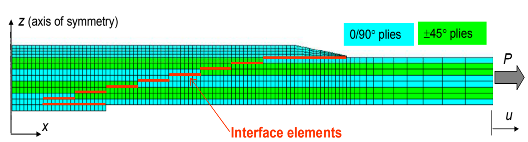

FIG. 30: Finite element model of stepped-joint repair specimen.

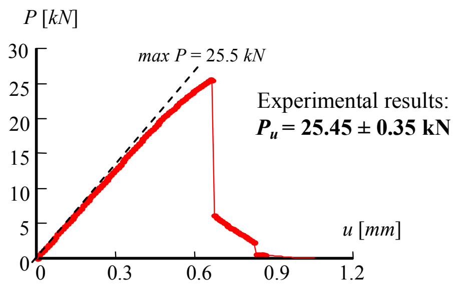

FIG. 31: Load versus end displacement from finite element analysis.

The fatigue damage parameter was derived from a formulation proposed by Peerlings et al.[24] where the influence of fatigue damage on the interface constitutive law may be seen in Figure 32.

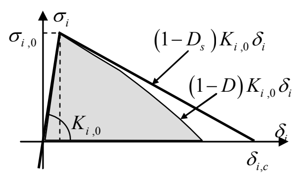

FIG. 32: Interface constitutive law showing influence of fatigue (i= I, II).

The damage parameter, D, is the sum of the static damage parameter, D_s and the fatigue damage parameter, D_f , which is given by:

(5) $$D_f = -\frac{1}{\lambda}\ln\left[1-\lambda Z N\right] \qquad \text{where } Z = \frac{C}{\beta+1}\left(\frac{\delta}{\delta_c}\right)^{(\beta+1)}$$

C, β and λ are material parameters and N is the number of cycles. Figure 33 shows that a suitable choice of these parameters yields excellent agreement with the experimental tests of stepped-joint repairs testing in fatigue. Further work is required to ascertain whether these values can indeed be regarded as material parameters for the adhesively-bonded repair.

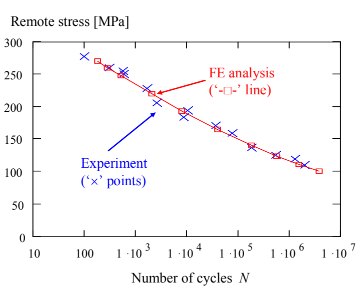

FIG. 33: Failure stress versus number of cycles.

4.6 Concluding remarks for Work Element 3

A number of experimental studies have been presented, by members of the consortium, which yield valuable insight into the evolution of damage in repaired composite structures. The use of finite element analysis is well established in the aerospace industry and the computational developments which have arisen form this work will provide analysts with improved capabilities for predicted the behaviour of repaired composite aerostructures under static and fatigue loading.

5. WE-4: FATIGUE

5.1 Introduction

The fourth work element was dedicated to investigating the fatigue of carbon-fibre primary structures. In general, these structures are not considered to be fatigue-critical since ultimate design strains are kept low (usually around 4000 microstrain). Fatigue certification requirements, though, results in the need to perform a large amount of tests, which is costly and time consuming. The first task of this programme was to produce a literature survey[25]. The second task was to collect existing experimental data as well as generating new test data for model calibration and validation. The final task was to develop predictive methodologies where two approaches were undertaken; one was simulating the fatigue behaviour of undamaged and in-plane pre-damaged composite laminates and structures (DLR) and the other was simulating delamination growth under fatigue loading (ONERA). It is hoped that this work will ultimately contribute to raising the design strain allowables in composite structures, thereby realising their full potential.

5.2 Fatigue and residual strength simulation (DLR - GERMANY)

The aim of this work was to develop efficient methodologies for predicting the in-plane fatigue behaviour of composites. Ideally the model should:

- only require a small number of experimental tests to deduce the necessary material parameters,
- not require a large computational effort,
- be validated experimentally by correctly capturing the fatigue-induced failure mechanisms.

A subroutine was implemented in the in-house finite element code, CODAC (see Section 2.5), where the in-plane residual strength degradation for a single ply was given by[26]:

(6) $$S_{ij}\left(n,\sigma_{ij},k\right) = \left[1-\left(\frac{\log(n)-\log(0.25)}{\log\left(N_{f_{ij}}(k)\right)-\log(0.25)}\right)^{\beta_{ij}}\right]^{\frac{1}{\alpha_{ij}}}\left(S_{ij}(0)-\sigma_{ij}\right)+\sigma_{ij}$$

where $S_{ij}(0)$ are the static strengths, σ_{ij} are the maximum applied stresses in the longitudinal, transverse and in-plane shear fatigue tests, k is the stress ratio, N_f is the corresponding number of cycles to failure and α_{ij} , β_{ij} are curve fitting parameters and i,j=1,2. This model considered fibre failure (1-direction) and matrix failure (2-direction) only (in-plane damage) and used the following interaction criteria:

(7) $$\left(\frac{\sigma_{ii}}{S_{ii}\left(n,\sigma_{ii},k\right)}\right)^2+\left(\frac{\sigma_{ij}}{S_{ij}\left(n,\sigma_{ij},k\right)}\right)^2-1=0$$

A number of tests to determine the material constants need to be undertaken and at the time of writing this paper, such tests had not yet been performed. The methodology, therefore, has yet to be validated. If the validation is successful, the experimental effort could be substantially reduced because the behaviour of the laminates could be deduced from the fatigue properties of unidirectional plies. This would enable a design engineer to tailor laminates for optimum fatigue performance without the necessity of performing fatigue tests for each laminate considered.

5.3 Delamination growth simulation under fatigue loading (ONERA - FRANCE)

The approach presented here is somewhat different from the one in Section 4.5. Delamination growth under fatigue loading was also based on the Paris Law[27] and given by:

(8) $$\frac{d(a\cdot\nu)}{dN}=C\big(G(a)\big)^{m}$$

where a is the crack displacement, ν is the unit normal to the delamination front directed toward the delaminated area, N is the number of cycles, G is the SERR, C and m are material parameters. Equation (8) is commonly solved numerically using either an explicit scheme as the Euler scheme, or an implicit scheme.

The first example is a DCB where isotropic material was assumed with E=150 GPa, an initial crack length a_0 = 30 mm, thickness of each arm, h = 1.5 mm with constants m = 3.74 and C = 5.154. Figure 34 shows the variation of the crack length extension $a - a_0$ with respect to the cycles number N for a constant increment ΔN = 4,000. Both the implicit scheme (Implicit) and the improved Euler scheme (Imp. Euler) gave results very close to the analytical solution. A computation made with ΔN = 20,000 (Figure35) shows the inefficiency of the explicit method whereas the implicit method gave good results.

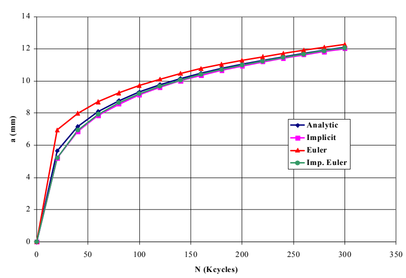

FIG. 34: Crack propagation as a function of number of cycles (ΔN = 4000).

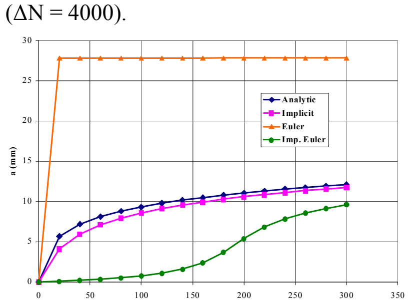

FIG. 35: Crack propagation as a function of number of cycles (ΔN = 20,000).

The second example is of a unidirectional circular plate with a radius of 80 mm and a thickness of 2 mm. A central circular delamination of 25 mm radius was inserted at the mid-plane. It was clamped at the edges and subjected to a cyclic loading with a maximum value of 100 N at the centre of both lower and upper surfaces. As in the previous case, the parameters of the Paris law were C = 5.174 and m = 3.74. The material properties used were E_L = 130,000 MPa, E_T = 9,500 MPa, ν_{LT} = 0.32, G_{LT} = 4,300 MPa (T300/914C). The computations were made with ΔN = 20,000. The results, after 200,000 cycles, are shown for both the Euler (Figure 36(a)) and Implicit (Figure 36(b)) schemes. The slight variations in the crack front obtained from these schemes was attributed to the smoothing algorithms, used in each solution scheme, to define the crack front.

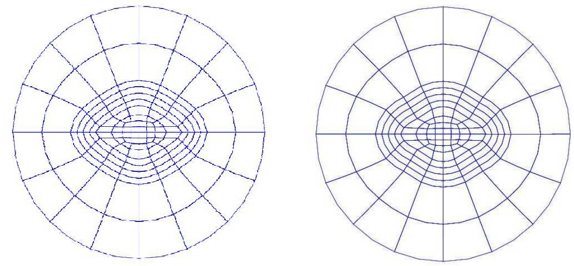

(a) (b)

FIG. 36: Crack growth using (a) Euler scheme and (b) Implicit scheme.

The final example is of a rectangular plate with a central circular delamination (10 mm diameter) at the second interface from the top ply and loaded in compression. It was made from T300/914C with stacking sequence [±5/+45/±5/-45/0/±85/0/-45/$\mp$5/+45/$\mp$5][28], simply-supported along its boundary and subjected to in-plane tension/compression loading on the vertical edges in Figure 37 (stress ratio = -1) with a peak load magnitude of 220 MPa. The location of the crack front at different values of N is shown in the Figure where the Euler scheme was used with small ΔN because of crack growth instability. This instability caused convergence difficulties within the implicit scheme. It was observed experimentally that the crack front initially propagated in the axial direction before progressing rapidly in the transverse direction and this was captured using the current analysis.

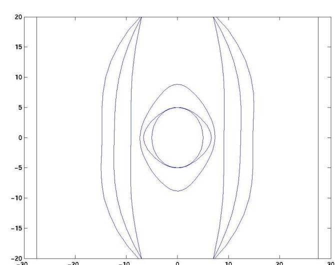

FIG. 37: Crack front location for different values of N.

5.4 Concluding remarks for Work Element 4

A methodology for predicting fatigue life and in-plane residual strength of composites was implemented by DLR in an efficient in-house finite element code, CODAC. This has yet to be validated and if successful, the experimental effort to characterise in-plane fatigue performance could be substantially reduced since the behaviour of laminates could be deduced from the fatigue properties of unidirectional plies. ONERA developed implicit and schemes for simulating delamination growth under fatigue loading and showed that both methods were robust for stable crack growth but recommended that an explicit scheme is used for unstable crack growth.

ACKNOWLEDGEMENT

A number of participants have made substantial and important contributions to this four-year research programme. The author is particularly indebted to Florence Roudolff, Yves Ousset, Alain Déom and Jaap Wiggenraad at ONERA; Serge Maison-Le Poec and Stéphan Guinard at EADS-CCR; Klaus Rohwer, Michael Gädke and Jens Baaran at DLR; Dieter Hachenberg at AIRBUS Deutschland; Josef Mendler and Deiter Pestal at EADS-M; Aniello Riccio at CIRA; Javier San Millan and Marcos Castañón Álvarez at INTA; Leif Asp at SICOMP; Tonny Nyman at SAAB; Ralf Creemers at NLR; Steve Lord and Andrew Davies at QinetiQ; Fadhil Habib at BAE Systems; Robin Olsson and Emile Greenhalgh at Imperial College London and Costas Soutis at The University of Sheffield.

REFERENCES

[1] Hull, D., Damage mechanism characterisation in composite damage tolerance investigations, Composite Structures, **23**, pp 99-120 (1993).

[2] Olsson, R., Impact Response and delamination of composite plates, PhD Thesis, Royal Institute of Technology (1998).

[3] Olsson, R., Donadon, M. V. and Falzon, B. G., Delamination threshold load for dynamic impact on plates, International journal of solids and structures, **43**, pp 3124-3141 (2006).

[4] Falzon, B. G., GARTEUR AG-28: Impact Damage and Repair of Composite Structures, GARTEUR, (2006).

[5] Bathe, K.-J., Finite element procedures, Prentice-Hall, Inc., New Jersey (1996).

[6] Choi, H. Y. and Chang, F. K., A model for predicting damage in graphite/epoxy laminated composites resulting from low-velocity point impact, Journal of composite materials, **26**, pp 2134-2169 (1992).

[7] Hashin, Z., Failure criteria for unidirectional fibre composites, Journal of Applied Mechanics, **47**, pp 329-334 (1980).

[8] Falzon, B. G., The behaviour of damage tolerant hat-stiffened composite panels loaded in uniaxial compression, Composites - Part A: Applied Science and Manufacturing, **32**, pp 1255-1262 (2001).

[9] Falzon, B. G. and Steven, G. P., Postbuckling behaviour of hat-stiffened thin-skinned carbon-fibre composite panels, Collection of Technical Papers - AIAA/ASME/ASCE/AHS/ASC Structures, Structural Dynamics & Materials Conference, New Orleans, LA, USA (1995).

[10] Falzon, B. G., Stevens, K. A. and Davies, G. O., Postbucking behaviour of a blade-stiffened composite panel loaded in uniaxial compression, Composites - Part A: Applied Science and Manufacturing, **31**, pp 459-468 (2000).

[11] Falzon, B. G., Stiffened composite panels loaded in uniaxial compression - database, CD, Imperial College London (2004).

[12] Rybicki, E. F. and Kanninen, M. F., A finite element calculation of stress intensity factors by a modified crack closure integral, Engineering Fracture Mechanics, **9**, pp 931-938 (1977).

[13] Crisfield, M. A., Non-linear finite element analysis of solids and structures-Volume 1, John Wiley & Sons Ltd, Chichester (1991).

[14] van der Veen, H., Vuik, K. and de Borst, R., Branch switching techniques for bifurcation in soil deformation, Computer Methods in Applied Mechanics and Engineering, **190**, pp 707-719 (2000).

[15] Romeo, G. and Frulla, G., Nonlinear analysis of anisotropic plates with initial imperfections and various boundary conditions subjected to combined biaxial compression and shear loads, International journal of solids and structures, **31**, pp 763-783 (1994).

[16] Falzon, B. G. and Hitchings, D., Capturing mode-switching in postbuckling composite panels using a modified explicit procedure, Composite Structures, **60**, pp 447-453 (2003).

[17] Charalambides, M. N., Hardouin, R., Kinloch, A. J. and Matthews, F. L., Adhesively-bonded repairs to fibre-composite materials I: experimental, Composites - Part A: Applied Science and Manufacturing, **29**, pp 1371-1381 (1998).

[18] Charalambides, M. N., Kinloch, A. J. and Matthews, F. L., Adhesively-bonded repairs to fibre-composite materials II: finite element modelling, Composites - Part A: Applied Science and Manufacturing, **29**, pp 1383-1396 (1998).

[19] Habib, F. A., A new method for evaluating the residual compression strength of composites after impact, Composite Structures, **53**, pp 309-316 (2001).

[20] Hu, F. Z. and Soutis, C., Strength prediction of patch-repaired CFRP laminates loaded in compression, Composites science and technology, **60**, pp 1103-1114 (2000).

[21] Soutis, C., Duan, D. M. and Goutas, P., Compressive behaviour of CFRP laminates repaired with adhesively bonded external patches, Composite Structures, **45**, pp 289-301 (1999).

[22] Tenchev, R. T. and Falzon, B. G., Experimental and numerical study of debonding in composite adhesive joints., 16th International Conference on Composite Materials, Kyoto, Japan (2007).

[23] Tenchev, R. T. and Falzon, B. G., A pseudo-transient solution strategy for the analysis of delamination by means of interface elements, Finite elements in analysis and design, **42**, pp 698-708 (2006).

[24] Peerlings, R. H. J., Brekelmans, W. A. M., de Borst, R. and Geers, M. G. D., Gradient-enhanced damage modelling of high-cycle fatigue, International Journal for Numerical Methods in Engineering, **49**, pp 1547-1569 (2000).

[25] Habib, F. A., Davies, A., Baaran, J. and Ousset, Y., Literature survey on fatigue behaviour of composite structures - GARTEUR AG-28, GARTEUR, TP-146 (2004).

[26] Adam, T., Dickson, R. F., Jones, C. J., Reiter, H. and Harris, B., A power law fatigue damage model for fibre-reinforced plastic laminates, Proceedings of the Institution of Mechanical Engineers, Part C: Mechanical Engineering Science, **200**, pp 155-166 (1986).

[27] Paris, P. and Erdogan, F., Critical analysis of crack propagation laws, American Society of Mechanical Engineers -- Transactions -- Journal of Basic Engineering, **85**, pp 528-534 (1963).

[28] Kruger, R., Hansel, C. and Konig, M., Experimental-numerical investigation of delamination buckling and growth, University of Stuttgart, Germany, NR 96/3 (1996).